

# Cooling curves and initial models for low-mass white dwarfs ( $< 0.25 M_{\odot}$ ) with helium core

Marek J. Sarna<sup>1</sup>, Ene Ergma<sup>2</sup> and Jelena Antipova<sup>2</sup>

<sup>1</sup> *N. Copernicus Astronomical Center, Polish Academy of Sciences, ul. Bartycka 18, 00-716 Warsaw, Poland.*

<sup>2</sup> *Physics Department, Tartu University, Ülikooli 18, EE2400 Tartu, Estonia.*

Accepted . Received ; in original form 1999

## ABSTRACT

We present a detailed calculation of the evolution of low-mass ( $< 0.25 M_{\odot}$ ) helium white dwarfs. These white dwarfs (the optical companions to binary millisecond pulsars) are formed via long-term, low-mass binary evolution. After detachment from the Roche lobe, the hot helium cores have a rather thick hydrogen layer with mass between 0.01 to 0.06  $M_{\odot}$ . Due to mixing between the core and outer envelope, the surface hydrogen content is 0.5 to 0.35, depending on the initial value of the heavy element (Z) and the initial secondary mass. We found that the majority of our computed models experience one or two hydrogen shell flashes. We found that the mass of the helium dwarf in which the hydrogen shell flash occurs depends on the chemical composition. The minimum helium white dwarf mass in which a hydrogen flash takes place is  $0.213 M_{\odot}$  (Z=0.003),  $0.198 M_{\odot}$  (Z=0.01),  $0.192 M_{\odot}$  (Z=0.02) or  $0.183 M_{\odot}$  (Z=0.03). The duration of the flashes (independent of chemical composition) is between few  $\times 10^6$  years to few  $\times 10^7$  years. In several flashes the white dwarf radius will increase so much that it forces the model to fill its Roche lobe again. Our calculations show that cooling history of the helium white dwarf depends dramatically on the thickness of the hydrogen layer. We show that the transition from a cooling white dwarf with a temporary stable hydrogen-burning shell to a cooling white dwarf in which almost all residual hydrogen is lost in a few thermal flashes (via Roche-lobe overflow) occurs between  $0.183$ – $0.213 M_{\odot}$  (depending on the heavy element value).

**Key words:** binaries: close — binaries: general — stars: mass loss evolution — stars: millisecond binary pulsars — pulsars: individual: PSR J0437 + 4715 — pulsars: individual: PSR J1012 + 5307

## 1 INTRODUCTION

Kippenhahn, Kohl & Weigert (1967) were the first who followed the formation of helium white dwarfs (WD) of low mass in a binary system. The evolution of a helium WD of  $0.26 M_{\odot}$  (remnant) was investigated by Kippenhahn, Thomas & Weigert (1968) who found that a hydrogen flash can be initiated near the base of the hydrogen rich envelope. The energy of the flash is sufficient to cause the envelope to expand to giant dimensions and hence it may be possible that another short term Roche lobe filling can occur.

In Webbink (1975), models of a helium white dwarf were constructed by formally evolving a model from the homogeneous zero-age main sequence with the reduction of the mass of the hydrogen-rich envelope. When the mass of the envelope is less than some critical value, the model contracts adopting white dwarf dimensions. Webbink found that ther-

mal flashes do not occur for WDs less massive than  $0.2 M_{\odot}$ . Alberts et al. (1996) have confirmed Webbink's finding that low-mass white dwarfs do not show thermal flashes and the cooling age for WDs of mass  $M_{wd} \leq 0.20 M_{\odot}$  can be considerably underestimated if using the traditional WD cooling curves which were constructed for  $M_{wd} > 0.3 M_{\odot}$  (Iben & Tutukov 1986, IT 86).

Recently, Hansen & Phinney (1998a – HP98) and Benvenuto & Althaus (1998 – BA98) investigated the effect of different mass of the hydrogen layer ( $10^{-8} \leq M_{env}/M_{\odot} \leq 4 \times 10^{-3}$ ) on the cooling evolution of  $0.15 \leq M_{He}/M_{\odot} \leq 0.5$  helium WDs. In both calculations (BA98 and HP98) the mass of the hydrogen envelope left on the top of white dwarf has been taken as free parameter. BA98 found that thick envelopes appreciably modify the radii and surface gravities of no-H models, especially in the case of low-mass helium white dwarfs.

Driebe et al. (1998 – DSBH98) present a grid of evolutionary tracks for low-mass white dwarfs with helium cores in the mass range from 0.179 to 0.414  $M_{\odot}$ . The tracks are based on a 1  $M_{\odot}$  model sequence extending from the pre-main sequence stage up to the tip of red giant branch. Applying large mass loss rates forced the models to move off the giant branch and evolve across the Hertzsprung–Russell diagram and down the cooling branch. They found that hydrogen flashes take place only for two model sequences, 0.234  $M_{\odot}$  and 0.259  $M_{\odot}$ , and for very low-mass WDs the hydrogen shell burning remains dominant even down to effective temperatures well below 10 000 K. According to our previous calculations (Ergma, Sarna & Antipova, 1998) we find that for a low-mass white dwarf with a helium core, which was formed during low-mass binary evolution (after detachment from the Roche lobe), the hydrogen layer left on the top of the helium core is much thicker ( $\sim 1-6 \times 10^{-2} M_{\odot}$  with  $X_{\text{surf}}$  ranging from 0.3 to 0.52) than used in cooling calculation by HP98 and BA98. Also in DSBH98 (see their Table 1), for the two lowest total remnant masses the envelope mass value is smaller than obtained in our calculations.

## 2 THE MAIN AIM

Low-mass helium white dwarfs are present in millisecond binary pulsars and double degenerate systems. This gives a unique opportunity to test the cooling age of the WD in a binary and, especially in the case of millisecond binary pulsars, allows for age determinations for neutron stars that are independent of their rotational history.

## 3 THE EVOLUTIONARY CODE

The evolutionary sequences we have calculated are comprised of three main phases:

- detached evolution lasting until the companion fills its Roche lobe on the time-scale  $t_d$ ;
- semi-detached evolution (non-conservative in our calculations) on the time-scale  $t_{sd}$ ;  $t_0 = t_d + t_{sd}$ ;
- a cooling phase of the WD on the time-scale  $t_{cool}$  (the final phase during which a system with a ms pulsar + low-mass helium WD is left behind). The total evolutionary time is  $t_{evol} = t_0 + t_{cool}$ .

The duration of the detached phase is somewhat uncertain; it may be determined either by the nuclear time-scale or by the much shorter time-scale of the orbital angular momentum loss owing to the magnetized stellar wind.

In our calculations we assume that the semi-detached evolution of a binary system is non-conservative, i.e. the total mass and angular momentum of the system are not conserved. We can express the total orbital angular momentum ( $J$ ) of a binary system as

$$\frac{\dot{J}}{J} = \frac{\dot{J}}{J} \Big|_{SML} + \frac{\dot{J}}{J} \Big|_{MSW} + \frac{\dot{J}}{J} \Big|_{GR}, \quad (1)$$

where the terms on the right hand side are due to: stellar mass angular momentum loss from the system, magnetic stellar wind braking, and gravitational wave radiation.

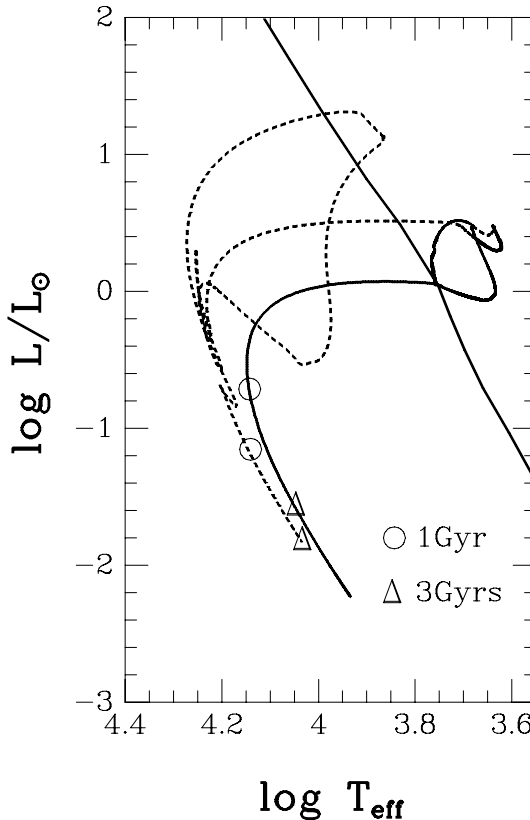


**Figure 1.** Hertzsprung–Russell diagram with evolutionary tracks. Evolutionary sequence (model 20) which undergoes long term stable hydrogen burning is shown by the solid line. Dashed line, the same for model 22 which shows one weak (without RLOF) and one strong (with RLOF) hydrogen flash. Circles and triangles mark cooling ages of 1 and 3 Gyr, respectively.

### 3.1 Stellar mass angular momentum loss

The formalism which we have adopted is described in Muslimov & Sarna (1993). We introduce the parameter  $f_1$  characterizing the loss of mass from the binary system and defined by the relations,

$$\dot{M} = \dot{M}_2 f_1 \quad \text{and} \quad \dot{M}_1 = -\dot{M}_2 (1 - f_1), \quad (2)$$

where  $\dot{M}$  is the mass-loss rate from the system,  $\dot{M}_2$  is the rate of mass loss from the donor (secondary) star and  $\dot{M}_1$  is the accretion rate onto the neutron star (primary). The matter leaving the system will carry off its intrinsic angular momentum in agreement with formula

$$\frac{\dot{J}}{J} \Big|_{SML} = f_1 f_2 \frac{M_1 \dot{M}_2}{M_2 \dot{M}} \quad \text{yr}^{-1}, \quad (3)$$

where  $M_1$  and  $M_2$  are the masses of the neutron star and donor star, respectively and  $M = M_1 + M_2$ . Here we have introduced the additional parameter  $f_2$ , which describes the efficiency of the orbital angular momentum loss from the system due to a stellar wind (Tout & Hall 1991). In our calculations we have  $f_2 = 1$  and  $f_1 = 1$ ; we calculate the fully non-conservative case, although additional calculations with  $f_1 = 0.9$  and  $0.5$  (with  $f_2 = 1$ ) give similar results. A similar result to ours was found by Tauris (1996), who showed

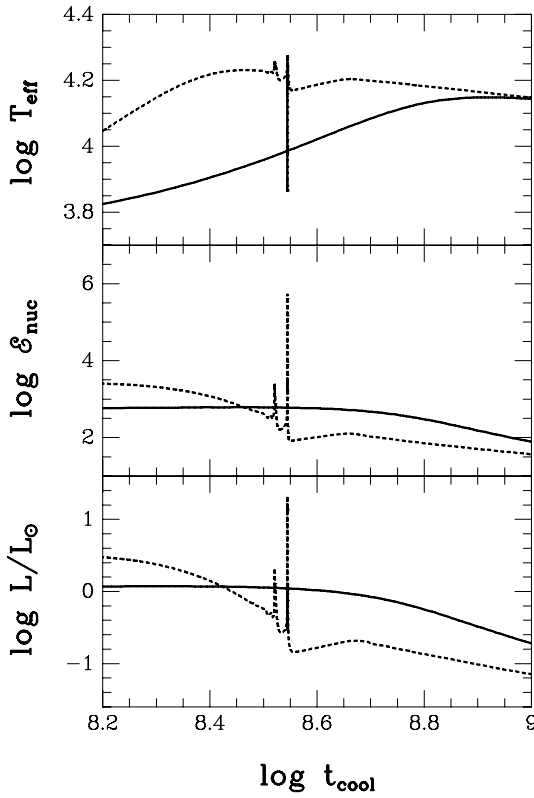


**Figure 2.** The surface effective temperature (upper panel), the nuclear energy production (middle panel) and the surface luminosity (lower panel) plotted as a function of the cooling time  $t_{cool}$  which is the time elapsed from  $t_0$ . Model 20 with stationary hydrogen shell burning – thick line  $t_0=7.9\times 10^9$  yrs, model 22 with unstable hydrogen shell burning – dashed line  $t_0=7.8\times 10^9$  yrs. First flash is without RLOF and second flash is accompanied by RLOF. For all figures with cooling time  $t_{cool}$  is time elapsed from  $t_0$ .

that the change in orbital separation due to mass transfer in LMXB (low-mass X-ray binaries) as a function of the fraction of exchanged matter  $f_1$  which is lost from system is small (for  $0.5 \leq f_1 \leq 1$ ). To understand whether the system evolution is conservative or non-conservative is not easy in the case of a rapidly rotating neutron star; no easy solution can be found. We propose as one possibility a factor which may help us to distinguish between the two cases – the surface magnetic field of the neutron star and its evolution during the accretion.

### 3.2 Magnetic stellar wind braking

We also assume that the donor star, possessing a convective envelope, experiences magnetic braking (Mestel 1968; Mestel & Spruit 1987; Muslimov & Sarna 1995), and, as a consequence, the system loses its orbital angular momentum. For a magnetic stellar wind we used the formula for the orbital angular momentum loss

$$\left. \frac{J}{J} \right|_{MSW} = -3 \times 10^{-7} \frac{M^2 R_2^2}{M_1 M_2 a^5} \text{ yr}^{-1}, \quad (4)$$

where  $a$  and  $R_2$  are the separation of the components and the radius of the donor star in solar units.

### 3.3 Gravitational wave radiation

For systems with very short orbital periods, during the final stages of their evolution we also take into account the loss of orbital angular momentum due to emission of gravitational radiation (Landau & Lifshitz 1971):

$$\left. \frac{J}{J} \right|_{GR} = 8.5 \times 10^{-10} \frac{M_1 M_2 M}{a^4} \text{ yr}^{-1} \quad (5)$$

The mass and accompanying orbital angular momentum loss from these system are poorly understood problems in the evolution of binary stars. As is well known, the variation of the angular momentum depends critically on the assumed model (Ergma et al. 1998). In the case of binary systems with ms pulsar typically two different models concerning the mass ejection and angular momentum loss can be adopted. The first is that the amount of angular momentum lost per 1 gram of ejected matter is equal to the average orbital angular momentum of 1 gram of the binary. The second is that the matter that flows from the companion star onto the neutron star (after accretion) is ejected isotropically with the specific angular momentum of the neutron star. In this paper, for our non-conservative approach we have adopted the first model. This affects significantly our results on the semi-detached evolution (see fig. 2 in Ergma et al. 1998), but very little changes the cooling time-scale of the helium white dwarf.

### 3.4 Illumination of the donor star

In all cases we have included the effect of illumination of the donor star by the millisecond pulsar. In our calculations we assume that illumination of the component by the hard (X-ray and  $\gamma$ -ray) radiation from the millisecond pulsar leads to additional heating of its photosphere (Muslimov & Sarna 1993). The effective temperature  $T_{eff}$  of the companion during the illumination stage is determined from the relation

$$L_{in} + P_{ill} = 4\pi\sigma R_2^2 T_{eff}^4, \quad (6)$$

where  $L_{in}$  is the intrinsic luminosity corresponding to the radiation flux coming from the stellar interior and  $\sigma$  is the Stefan-Boltzmann constant.

$P_{ill}$  is the millisecond pulsar radiation that heats the photosphere, which is determined by

$$P_{ill} = f_3 \left( \frac{R_2}{2a} \right)^2 L_{rot} \quad (7)$$

and  $L_{rot}$  is “rotational luminosity” of the neutron star due to magneto-dipole radiation (plus a wind of relativistic particles)

$$L_{rot} = \frac{2}{3c^3} B^2 R_{ns}^6 \left( \frac{2\pi}{P_p} \right)^4, \quad (8)$$

where  $R_{ns}$  is the neutron star radius,  $B$  is the value of the magnetic field strength at the neutron star and  $P_p$  is the pulsar period.  $f_3$  is the factor characterizing the efficiency of transformation of irradiation flux into thermal energy (in

our case we take  $f_3 = 2 \times 10^{-3}$ ). Note that in our calculations the effect of irradiation is formally treated by means of modification of the outer boundary condition, according to relation (6).

In this paper we do not follow the magnetic field and pulsar period ( $P_p$ ) evolution, as we did in our earlier papers (Muslimov & Sarna 1993, Ergma & Sarna 1996). We were mainly interested in finding initial models for low-mass helium white dwarfs and in investigating the initial cooling phase of these low-mass helium white dwarfs. From earlier calculations we know that if the magnetic field strength is greater than about  $10^9$  G, the neutron star spins-up to tenths and hundreds of milliseconds, rather than several milliseconds. This leads to a situation where the pressure of the magneto-dipole radiation is insufficient to eject matter from the system. Also from our previous calculations (see for example Ergma & Sarna 1996) we find that after accretion of a maximum of about  $0.2 M_\odot$ , the neutron star has spun-up to millisecond periods if  $B < 10^9$  G. Therefore in this paper we accept that after accretion of  $0.2 M_\odot$  the neutron star spins-up to about 2 ms. After spin-up the pulsar irradiation is strong enough to prevent accretion, and at this moment we include non-conservative mass loss from the system as described above.

During the initial high mass accretion phase ( $\dot{M}_2 \sim 10^{-8} - 10^{-9} M_\odot \text{ yr}^{-1}$ ,  $t_{\text{acc}} \sim 10^7 - 10^8$  yrs) the system may be observed as a bright low-mass X-ray binary (LMXB). It is necessary to point out that majority of LMXBs for which orbital period determinations are available (21 systems out of 24 according to van Paradijs catalogue 1995), have orbital period of less than one day. These systems therefore cannot be the progenitors of the majority of low-mass helium white dwarf + millisecond pulsar binary systems. A lack of LMXB systems with orbital period between 1 – 3 days does not allow us to make a direct comparison between the observational data and the results of our calculations.

### 3.5 The code

The models of the stars filling their Roche lobes were computed using a standard stellar evolution code based on the Henyey-type code of Paczyński (1970), which has been adapted to low-mass stars. The Henyey method involves iteratively improving a trial solution for the whole star. During each iteration, corrections to all variables at all mesh points in the star are evaluated using the Newton–Raphson method for linearised algebraic equations (see for example Hansen & Kawaler 1994). The Henyey method extended to calculate stellar evolution with mass loss, as adopted here, is well explained by Ziolkowski (1970). We note here that our code makes use of the stationary envelope technique, which was developed early on in the life of our code in order to save disc space (Paczyński 1969). This method makes the assumption that the surface 0.5 – 5% (by mass) of the star is not significantly affected by nuclear processes, such that it can be treated to a good approximation as homogeneous region (in composition) throughout the whole evolutionary calculation. During the cooling phase we assume that the static envelope is the surface 0.5% of the star. This assumption is valid during the flashes because the time-scale is longer than thermal time-scale of the envelope. We tested the possibility that the algorithm for redistributing mesh-

points introduces numerical diffusion into the composition profile. We find that if such numerical diffusion is real, it has only a marginal influence on the hydrogen profile. We would also like to note that in the heat equation we neglect the derivative with respect to molecular weight, since its effect is small. Convection is treated with the mixing-length algorithm proposed by Paczyński (1969). We solve the problem of radiative transport by employing the opacity tables of Iglesias & Rogers (1996). Where the Iglesias & Rogers (1996) tables are incomplete, we have filled the gaps using the opacity tables of Huebner et al. (1977). For temperatures less than 6000 K we use the opacities given by Alexander & Ferguson (1994) and Alexander (private communication). The contribution from conduction present in the opacity tables of Huebner et al. (1977) has been included by us in the other tables, since they don't include it (Haensel, private communication). The equation of state (EOS) includes radiation and gas pressure, which is composed of the ion and electron pressure. Contribution to the EOS owing to the non-ideal effects of Coulomb interaction and pressure ionization which influence the EOS, as discussed by Pols et al. (1995), have not been included in our program, and for this reason we stopped our cooling calculations before these effects become important. During the initial phase of cooling, the physical conditions in the hot white dwarfs are such that these effects are usually small.

## 4 EVOLUTIONARY CALCULATIONS

We perform our evolutionary calculations for binary systems initially consisting of a  $1.4 M_\odot$  neutron star (NS) and a slightly evolved companion (subgiant) of two masses, 1 and 1.5, and four chemical compositions (Z: 0.003, 0.01, 0.02, 0.03). We have produced (Table 1) a number of evolutionary tracks corresponding to the different possible values of the initial orbital period (ranging from 0.7 to 3.0 days) at the beginning of mass transfer phase.

## 5 THE RESULTS

In Table 1 we list the characteristic of the cooling phase of the WD,  $t_{\text{cool}}$ , and the maximum possible evolution time of a system,  $t_{\text{evol}}$ , which is a sum of times of detached (determined by nuclear evolution), semi-detached, and cooling phases. The cooling is the last phase of evolution of the WD, and in our calculations starts at the end of RLOF. The cooling time,  $t_{\text{cool}}$ , is limited to an initial cooling stage during which the WD cools until its central temperature has decreased by 50 % of its maximum value. From Table 1 it is clearly seen that to produce short orbital period systems in a time-scale shorter than Hubble time it is necessary either to have low Z or a more massive secondary.

In our calculations the donor star fills its Roche lobe while it is evolving through the Hertzsprung gap, and therefore it transfers mass on its companion in a thermal time-scale.

Figure 1 shows the evolutionary cooling sequences for models 20 and 22 (more details in Table 1). Model 20 presents the case with stable hydrogen burning. Model 22

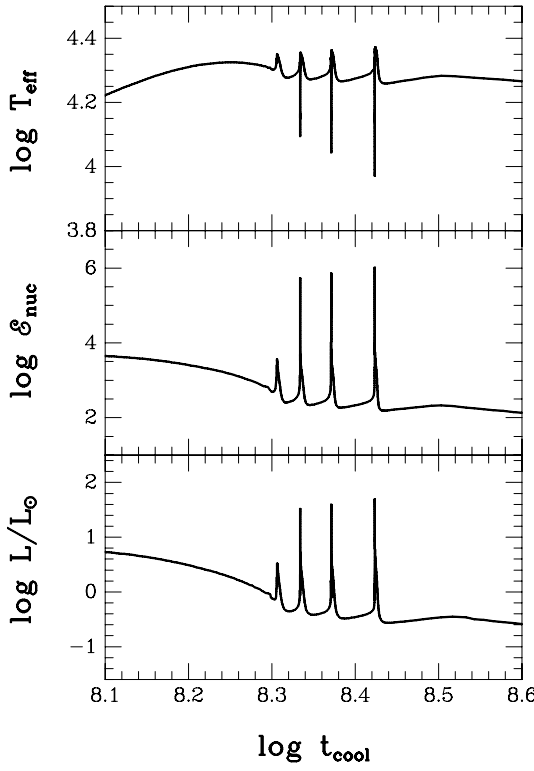


**Figure 3.** Hydrogen flashes on a helium WD of mass  $0.213 M_{\odot}$  (model 7) which show four flashes without RLOF. The curves present the effective temperature (upper panel), nuclear energy production in the hydrogen burning shell (middle panel) and the luminosity (lower panel) as a function of cooling time,  $t_0=5.2 \times 10^9$  yrs.

shows the case when the thermal instability of the hydrogen–burning shell occurs. The first flash is not strong enough to allow the star to overflow its Roche lobe, but during the second flash the radius of the secondary increases to fill its Roche lobe and short–time Roche lobe overflow (RLOF) occurs.

In Table 2 we present the mass–radius relationship for WDs from our calculations, DSBH98, the Wood models, and the Hamada & Salpeter (1961) zero–temperature helium WD models calculated for a surface temperature of 8500 K (as in van Kerkwijk, Bergeron & Kulkarni 1996 for PSR1012+5307). Comparison of the numbers demonstrate that for WD masses of  $< 0.25 M_{\odot}$ , the results of our calculations differ significantly from a simple extrapolation obtained from the cooling curves (Wood 1990) performed for carbon WDs with the thick hydrogen envelopes. In addition comparing the cooling time–scales of HP98 and BA98 with those of Webbink and our models, shows differences of an order of magnitude (Table 3) for WD masses of  $< 0.25 M_{\odot}$ .

## 6 HYDROGEN FLASH BURNING

The problem of unstable hydrogen shell burning in low–mass helium WDs was first discussed in the literature more than 30 years ago (Kippenhahn, Thomas & Weigert 1968). Recently, Alberts et al. (1996) have claimed that they do

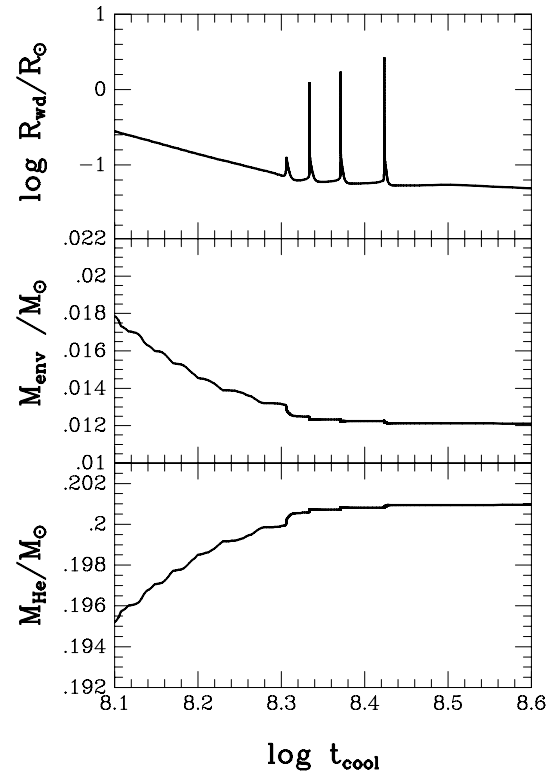


**Figure 4.** Hydrogen flashes on a helium WD of mass  $0.213 M_{\odot}$  (model 7). The curves present the white dwarf radius (upper panel), the envelope mass (middle panel) and the mass of the helium core (lower panel) as a function of the cooling time,  $t_0=5.2 \times 10^9$  yrs.

not see any thermal flashes that result from thermally unstable shell–burning, as reported in papers IT86 and Kippenhahn, Thomas & Weigert (1968). Webbink (1975) found that in none of his model sequences, such a severe thermal runaway as described by Kippenhahn et al. (1968) was found, although mild flashes for  $M > 0.2 M_{\odot}$  did take place. Alberts et al. found that even reducing the time step to 50–100 years would not lead to thermally unstable shell–burning for  $M_{wd} < 0.25 M_{\odot}$ . In DSBH98, thermal instabilities of the hydrogen–burning shell occurs in their two models,  $0.234 M_{\odot}$  and  $0.259 M_{\odot}$ . They concluded that hydrogen flashes take place only in the mass interval  $0.21 \leq M/M_{\odot} \leq 0.3$ .

According to our computations, low–mass helium WDs with masses more than  $0.183 M_{\odot}$  ( $Z=0.03$ ),  $0.192 M_{\odot}$  ( $Z=0.02$ ),  $0.198 M_{\odot}$  ( $Z=0.01$ ) and  $0.213 M_{\odot}$ , ( $Z=0.003$ ) may experience up to several hydrogen flashes before they enter the cooling stage. In Table 4 we present several characteristics for the computed flashes. We discuss two kinds of flashes: in the first case (in Table 4 shown as “1”), during the flash the secondary does not fill its Roche lobe i.e. the mass of the white dwarf does not change, and in the second case (“2”), during the unstable hydrogen burning phase the secondary fills its Roche lobe and the system again enters into a very short duration accretion phase (see Table 4). We introduce four time–scales to describe the flash behaviour: (i) the flash rise time–scale  $\Delta t_1$ , which is the time for the luminosity to increase from minimum to maximum value

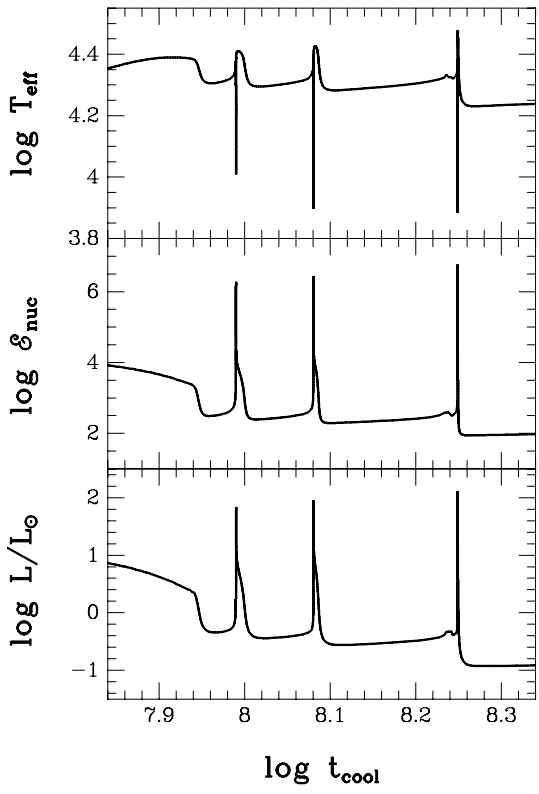


**Figure 5.** Same as for Fig.3 but for model 17. During first flash the secondary does not fill its Roche lobe but during the second and third flashes RLOF occurs and the total mass of white dwarf decreases ( $t_0 = 1.4 \times 10^9$  yrs).

(typically this value is between few  $\times 10^6$  to few  $\times 10^7$  yrs – third column in the Table 4); (ii) the flash decay time-scale  $\Delta t_2$ , which is the time for the luminosity to decrease to the initial value (typically from few hundred thousand to few tenth million years); (iii)  $\Delta T$  is the recurrence time between two successive flashes (iv)  $\Delta t_{acc}$  is the duration of the accretion phase when the secondary fills its Roche lobe during hydrogen shell flash.

For all sequences with several unstable hydrogen shell burning stages (usually for case “1”), the first flash is the weakest. In the majority of cases when the flash forces the star to fill its Roche lobe, only one flash takes place. For four cases we found two successive flashes with Roche lobe overflow (models 17, 23, 24, 31), and for another two cases (models 47, 53) to the first flash is not powerful enough to force the secondary fill its Roche lobe, but during the second flash it is.

How does the hydrogen flash burning influence the cooling time-scale? In Fig.2, the luminosity and nuclear energy production rates versus cooling time for models 20 and 22 are shown. Model 20 shows stationary hydrogen burning and model 22, hydrogen flash burning. Although before flash model 22 was more luminous than model 20, later the situation is reversed. After the flash, the burning mass of the hydrogen rich envelope in model 22 has decreased to  $0.0116 M_\odot$ , whereas the mass of the hydrogen envelope in model 20, in which stationary hydrogen burning occurs, is almost twice as large ( $0.0241 M_\odot$ ). If we look at how the

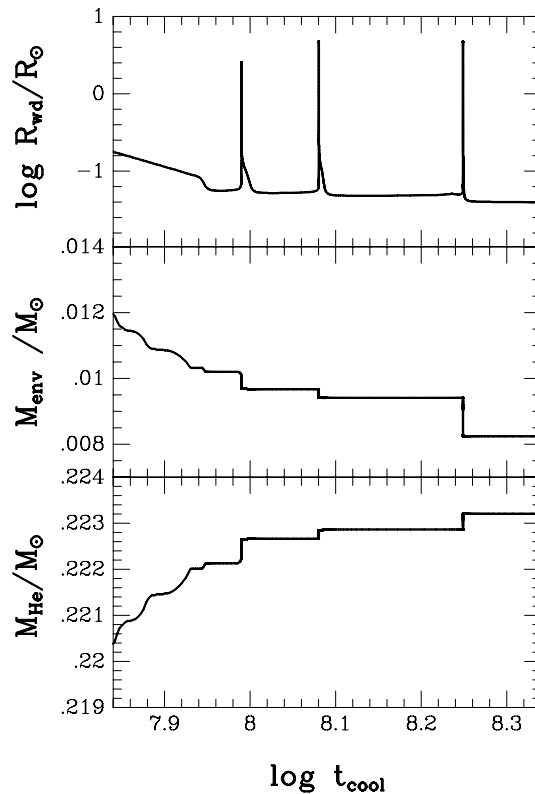


**Figure 6.** Same as for Fig.4 but for model 17. During the first flash the secondary does not fill its Roche lobe but during the second and third flashes RLOF occurs and the total mass of white dwarf decreases ( $t_0 = 1.4 \times 10^9$  yrs).

maximum nuclear energy rate behaves with cooling time, we can see that after the flash in model 22, the maximum energy production rate is less than in model 20 (stationary hydrogen burning).

In Fig. 3 we present the behaviour of  $\log T_{eff}$ ,  $\log \epsilon_{nuc}$  and  $\log L/L_\odot$ , and in Fig.4  $\log R_{wd}$ ,  $M_{env}$  and  $M_f/M_\odot$  as a function of cooling time for model 7. Before the helium white dwarf enters the final cooling phase, four unstable hydrogen flash burnings occur. The same parameters for model 17 (with RLOF) are shown in Figs. 5 and 6.

To investigate in more detail how the flashes develop, we show in Fig. 7 the evolution of the white dwarf radius (upper panel), nuclear energy generation rate (upper middle panel), maximum shell temperature and central temperature (lower middle panel) and the surface luminosity (lower panel) as a function of computed model number. In Fig. 7, as vertical dashed lines we marked several time-scales which characterize the flash behaviour (for numbers see Table 4).  $\Delta t_1$  and  $\Delta t_2$  describe the rise and decay times; the first characterizes the nuclear shell burning time-scale ( $\tau_{nuc}^{shell}$ ), the second the Kelvin–Helmholtz (thermal) envelope time-scale modified by nuclear shell burning ( $\Delta t_2 = \sqrt{\tau_{K-H}^{env} \tau_{nuc}^{shell}}$ ). The accretion time ( $\Delta t_{acc}$ ) is described by the square of the Kelvin–Helmholtz time-scale. The radiative diffusion time is defined as the Kelvin–Helmholtz time-scale of the extended envelope above the shell ( $\Delta t_{rd} = \tau_{K-H}^{env}$ ). The shape of the first flash on Fig. 7 shows some characteristic changes which are connected with physical processes in the stellar interior.

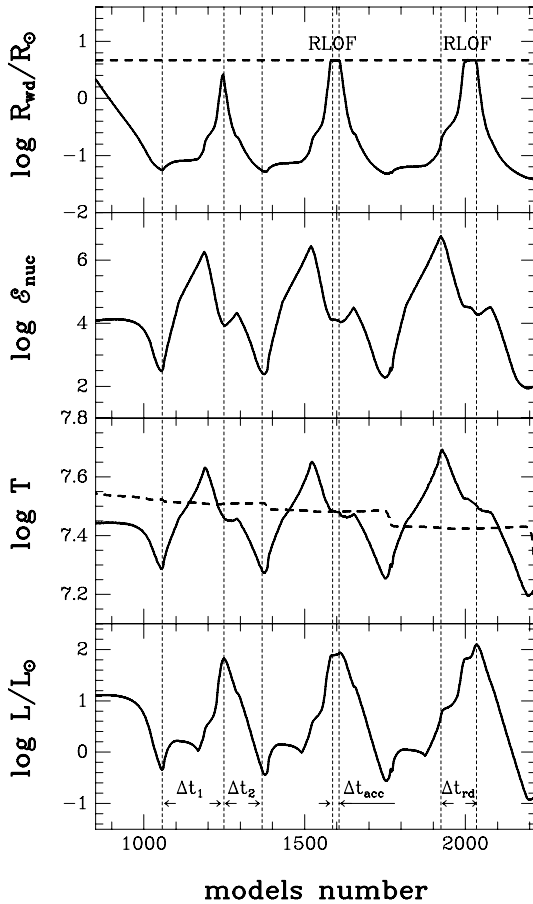


**Figure 7.** Hydrogen flashes on a helium WD of model 17. The white dwarf radius (solid line) together with Roche lobe radius (dashed line) (upper panel) the nuclear energy production in the hydrogen burning shell (upper middle panel) the maximum shell temperature (solid line) and central temperature (dashed line) (lower middle panel) and the surface luminosity (lower panel) as a function of model number are shown. The vertical lines define different time-scales during the flashes.

At the beginning of the flash the luminosity increases due to the more effective hydrogen burning in the shell source. After reaching a local maximum, the luminosity then decreases while the nuclear energy generation rate is still increasing rapidly. This decrease of the surface luminosity is due to a temperature inverting forming below the hydrogen shell. The energy generated in the hydrogen shell splits into two fluxes; coming outwards and going inwards. The helium core is heated effectively by the shell nuclear source – the central temperature increases by 2%. On Fig. 8 the evolution of the luminosity and temperature profiles during the  $\Delta t_1$  and  $\Delta t_2$  phases are shown. We clearly see how the inversion profile evolves and how the luminosity wave moves into the surface.

The nuclear energy generation rate in the shell has a maximum value far away from maximum surface luminosity. This is because the luminosity front is moving towards the stellar surface in a time-scale described by radiative diffusion ( $\Delta t_{rd}$ ). After reaching a maximum value, the luminosity starts to decrease and the energy generation rate also declines in the hydrogen shell over a time-scale  $\Delta t_2$  (for a

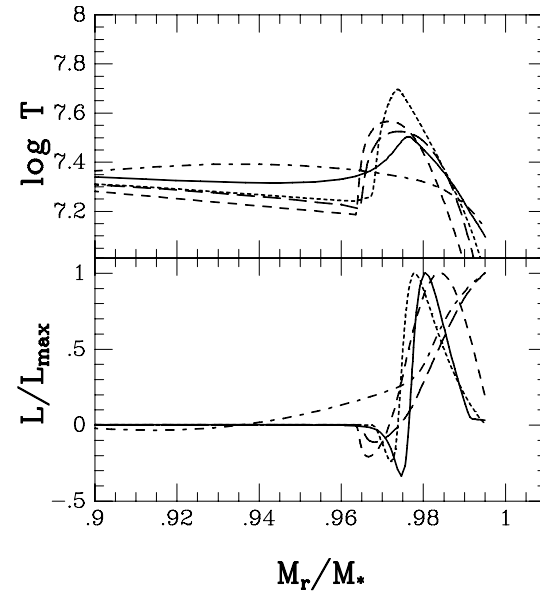


**Figure 8.** The evolution of temperature inversion layers and luminosity profile during a hydrogen flash. The evolutionary sequences are as follow: solid line – local luminosity minimum; dashed line – maximum temperature of the hydrogen shell; short dashed line – luminosity front moves outwards; long dashed line – maximum luminosity; dashed dotted line – decline of luminosity, heated core cooling effectively.

contracting envelope) the luminosity decreases to the minimum value. During the first flash, the stellar radius does not fill the inner Roche lobe. In the second and third flashes we have short episodes of super-Eddington mass transfer (see Table 4). During the RLOF phase, the orbital period slightly increases and the subgiant companion evolves quickly from spectral type F0 to A0.

As already pointed out, for several cases the secondary fills its Roche lobe and the system enters an accretion phase. During RLOF, the mass accretion rate is about three orders of magnitude greater than the Eddington limit (Fig. 9). All the accreted matter will be lost from the system ( $\Delta M_{acc} \sim 0.0001 - 0.001 M_\odot$ ). The accretion phase is very short, usually less than 1000 years (ranging from 160 to 2500 yrs – see Table 4). During the short super-Eddington accretion phase the system is a very bright X-ray source, with orbital period between 2 to 8 days.

We notice that during the flash the evolutionary time step strongly decreases and may be as short as several years.

## 7 ROLE OF BINARITY IN THE COOLING HISTORY OF THE LOW-MASS WHITE DWARF

DSBH98 modelled single star evolution and produced white dwarfs with various masses by applying large mass loss rates at appropriate positions in the red-giant branch to force the models to move off the giant branch. To show how binarity influences the final fate of the white dwarf cooling, we have computed extra sequences ( $1.0 + 1.4 M_\odot$ ,  $Z=0.02$ ,  $P_i=2.0$  days) where we did not take into account that the

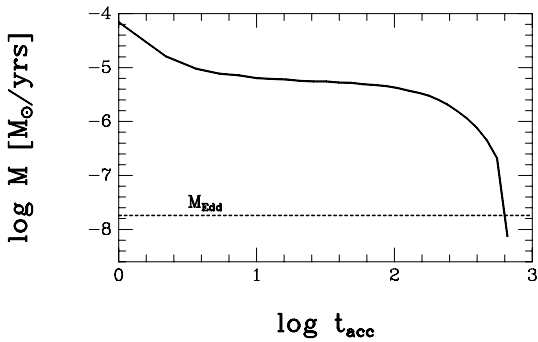


**Figure 9.** Mass accretion rate (model 42) versus time during a hydrogen shell flash with RLOF

star is in a binary system e.g. during hydrogen shell flash we do not allow RLOF. In complete binary model calculation, only one shell flash occurs accompanied with RLOF, whereas for the single star model calculation, four hydrogen shell flashes take place. Due to RLOF, the duration of the flash phase is  $2.7 \times 10^6$  yrs; if we do not include binarity the duration of the flash phase is  $1.8 \times 10^8$  yrs. However, the cooling time for helium white dwarfs less massive than  $0.2 M_\odot$  is not significantly changed. This is because the duration of flash phase is very short in comparison to the normal cooling phase (towards the white dwarf region). However, the effect of binarity will be important for the cooling history of more massive helium white dwarfs. In Fig. 10 both cases of evolution on the Hertzsprung–Russell diagram are shown – on the left panel Roche lobe overflow is not allowed, on right panel RLOF takes place.

## 8 APPLICATION TO INDIVIDUAL SYSTEMS

Below we discuss the observational data for several systems for which results of our calculations may be applied, by taking into account the orbital parameters of the system, the pulsar spin–down time, and the white dwarf cooling timescale.

### 8.1 PSR J0437–4715

Timing information for this millisecond binary system:  $P_p=5.757$  ms,  $P_{orb}=5.741$  days,  $\tau$  (intrinsic characteristic age of pulsar) = 4.4 – 4.91 Gyrs, mass function  $f(M)=1.23910^{-3} M_\odot$  (Johnston et al. 1993; Bell et al. 1995). Hansen & Phinney (1998b) have discussed the evolutionary stage of this system using their own cooling models described in HP98. They found consistent solution for all masses in the range  $0.15$  –  $0.375 M_\odot$  with thick (in the terminology of HP98) hydrogen envelopes of  $3 \times 10^{-4} M_\odot$ .

Timing measurements by Sandhu et al. (1997) have detected a rate of change in the projected orbital separation  $a \sin i$ , which they interpret as a change in  $i$  and they calculate for an upper limit for  $i < 43^\circ$  and new lower limit to the mass of the companion of  $M \sim 0.22 M_\odot$ . Our calculations also allow us to produce the orbital parameters and secondary mass for the PSR J0437–4715 system and fit its cooling age (2.5–5.3 Gyrs, Hansen & Phinney, 1998b), and

we find that the secondary fills its Roche lobe when the orbital period  $P_i$  is  $\sim 2.5$  days (Tables 1, 4). From our cooling tracks for a binary orbital period of 5.741 days, the mass of the companion is  $0.21 \pm 0.01 M_\odot$  and its cooling age 1.26–2.25 Gyrs (for a Population I chemical composition). These cooling models usually have one strong (with RLOF) hydrogen shell flash, after which the helium WD enters the normal cooling phase.

### 8.2 PSR J1012+5307

Lorimer et al. (1995) determined a characteristic age of the radio pulsar to be 7 Gyr, which could be even larger if the pulsar has a significant transverse velocity (Hansen & Phinney 1998b). Using the IT86 cooling sequences, they estimated the companion to be at most 0.3 Gyr old. HP98 models yield the following results for this system: the companion mass lies in the range  $0.13$ – $0.21 M_\odot$  and the WD age is  $< 0.6$  Gyr, the neutron star mass in the range  $1.3$ – $2.1 M_\odot$ .

Alberts et al. (1996) were the first to show that the cooling timescale of a low–mass WD can be substantially larger if there are no thermal flashes which lead to RLOF and a reduction of the hydrogen envelope mass. Our and DSBH98 calculations confirmed their results that for low–mass helium WDs ( $< 0.2 M_\odot$ ), indeed stationary hydrogen burning plays important role. To produce short (less than one day) orbital period systems with a low–mass helium WD and a millisecond pulsar it is necessary that the secondary fills its Roche lobe between  $P_{bif}$  and  $P_b$  (Ergma, Sarna & Antipova, 1998). If the initial orbital period  $P_i$  (at RLOF) is less than  $P_{bif}$ , the binary system evolves towards short orbital periods.  $P_b$  is another critical orbital period value. If  $P_b < P_i(\text{RLOF}) < P_{bif}$ , then a short orbital period ( $< 1$  day) millisecond binary pulsar with low–mass helium white dwarf may form. So the initial conditions of the formation of such systems are rather important. We calculated one extra sequence to produce a binary system with orbital parameters similar to PSR J1012+5307. Initial system:  $1 + 1.4 M_\odot$ ,  $P_i(\text{RLOF}) = 1.35$  days,  $Z=0.01$ . Final system :  $M_s=0.168 M_\odot$ ,  $P_f=0.605$  days,  $M_{env}=0.041 M_\odot$ . In Fig. 11 in the effective temperature and gravity diagram we show the cooling history of this white dwarf after detachment of the Roche lobe. The two horizontal regions are the gravity values inferred by van Kerkwijk et al. (1996) (lower) and Callanan et al. (1998) (upper). Our results are consistent with the Callanan et al. (1998) estimates. It is necessary to mention that after detachment from its Roche lobe, the outer envelope is rather helium–rich. Bergeron et al. (1991) have shown that a small amount of helium in a hydrogen–dominated envelope can mimic the effect of a larger gravity.

## 9 DISCUSSION

The results of our evolutionary calculations differ from those of Iben & Tutukov (1986) and Driebe et al. (1998) because of the different formation scenarios for low–mass helium WDs. In IT86’s calculations a donor star fills its Roche lobe while it is on the red giant branch (i.e. has a thick convective envelope) with a well developed helium core and a thin hydrogen burning layer. They proposed that the mass transfer time scale is so short that the companion will not be able

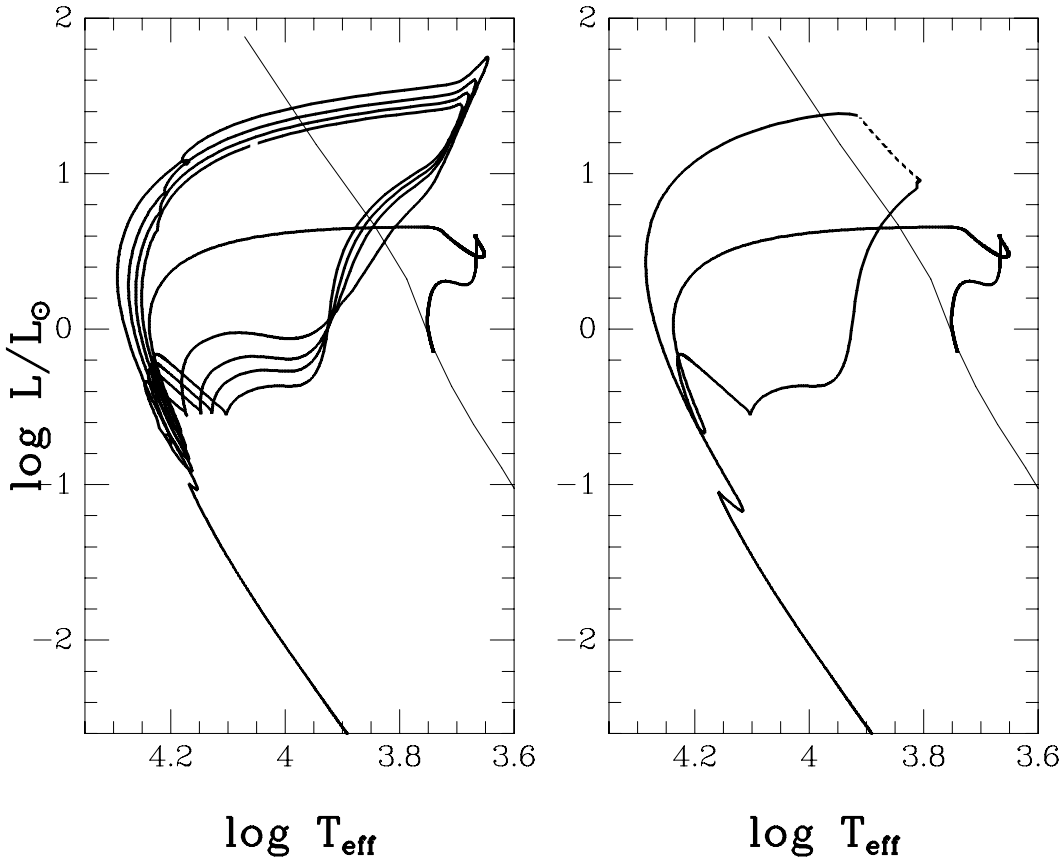


**Figure 10.** Hertzsprung–Russell diagram with evolutionary tracks. Evolutionary sequence  $1+1.4 M_{\odot}$ ,  $Z=0.02$ ,  $P_i=2.0$  days. Left panel RLOF is not allowed, right panel with RLOF.

to accrete the transferred matter and will itself expand and overflow its Roche lobe. The final output is the formation of a common envelope and the result of this evolution is a close binary with a helium WD of mass  $0.298 M_{\odot}$  having a rather thin ( $1.4 \times 10^{-3} M_{\odot}$ ) hydrogen-rich ( $X=0.5$ ) envelope.

DSBH98 did not calculate the mass exchange phases during the red giant branch evolution in detail but they also simulated the mass-exchange episode by subjecting a red giant branch model to a sufficiently large mass loss rate. In both cases (IT86 and DSBH98) mass loss starts when the star (with a well developed helium core) is on the red giant branch.

In our calculations the Roche lobe overflow starts when the secondary has either almost exhausted hydrogen in the center of the star or has a very small helium core with a thick hydrogen burning layer. During the semi-detached evolution the mass of the helium core increases from almost nothing to final value (for more detail about evolution of such systems, see Ergma, Sarna & Antipova, 1998). This is the reason that a much thicker ( $\sim [1.5 - 6] \times 10^{-2} M_{\odot}$ , with  $X$  ranging from 0.30 to 0.52) hydrogen-rich envelope is left on the donor star at the moment it shrinks within the Roche lobe.

The second important point where our results differ from that of DSBH98 is that in our calculations we can produce (after the secondary detaches from its Roche lobe) final millisecond binary pulsar parameters which we compare with observational data (orbital period, spin period of

ms pulsar, mass of the companion). It was shown by Joss, Rappaport & Lewis (1987) and more recently by Rappaport et al. (1995) that the evolution of a binary system initially comprising of a neutron star and a low-mass giant will end up as a wide binary containing a radio pulsar and a white dwarf in a nearly circular orbit. The relation between the white dwarf mass and orbital period (see eq. (6) in Rappaport et al. 1995) shows that if the secondary fills its Roche lobe while on the red giant branch, then for  $M_{wd} \approx 0.19 M_{\odot}$  the final orbital period would be  $\sim 5$  days, which is far from observed orbital period of the binary pulsar PSR J 1012+5307 ( $P_{orb}=0.6$  days).

Alberts et al. (1996), DSBH98, and the results of our calculations demonstrate clearly that especially for low-mass helium WDs ( $< 0.2 M_{\odot}$ ) stationary hydrogen burning remains an important, if not the main, energy source. HP98 and BA98 did consider nuclear burning but found it to be of little importance since their artificially chosen hydrogen envelope mass was less than some critical value, disallowing significant hydrogen burning. If we compare now the cooling curves of HP98, DSH98 with ours then there is one very important difference; they did not model the evolution of the helium WD progenitor and all their cooling models (see for example Figs. 11, 12 in HP98) start with a high  $T_{eff}$ . In our models, cooling of the helium WD starts after detachment of the secondary from its Roche lobe (DSBH98 mimic this situation with mass loss from the star). This time, the sec-

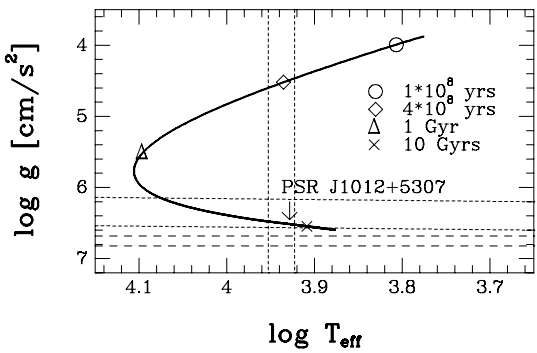


**Figure 11.**  $\log g - \log T_{\text{eff}}$  diagram with  $M_{\text{wd}} = 0.168 M_{\odot}$ . The arrow marks the position of the PSR J1012+5307 white dwarf. Two horizontal regions are the gravity values inferred by Callanan et al. (1998) (upper) and van Kerkwijk et al. (1996) (lower). The vertical lines show effective temperature constraints of Callanan et al. (1998)

secondary (proto-white dwarf) has rather low effective temperature (see for example Fig.1). During the evolution with  $L$  approximately constant, the effective temperature increases to a maximum value, after which it decreases while still having a active hydrogen shell burning source. The evolutionary time needed for the proto-white dwarf to travel from the minimum  $T_{\text{eff}}$  (after detachment from Roche lobe) to maximum  $T_{\text{eff}}$  depends strongly on mass of the WD (for a smaller mass a longer evolutionary time-scale).

So for low-mass helium WDs the evolutionary prehistory plays a very important role in cooling history of the white dwarf.

## 10 CONCLUSION

We have performed comprehensive evolutionary calculations to produce a close binary system consisting of a NS and a low-mass helium WD.

We argue that the presence of a thick hydrogen layer changes dramatically the cooling time-scale of the helium white dwarf ( $< 0.25 M_{\odot}$ ), compared to the previous calculations (HP98, BA98) where the mass of the hydrogen envelope was chosen as free parameter and was usually one order of magnitude less than that obtained from real binary evolution computations.

Also, we have demonstrated that using new cooling tracks we can consistently explain the evolutionary status of the binary pulsar PSR J1012+53.

Tables with cooling curves are available on <http://www.camk.edu.pl/~sarna/>.

## ACKNOWLEDGMENTS

We would like to thank Dr. Katrina M. Exter for help in improving the form and text of the paper. We would like to thank our referee Dr. Peter Eggleton for very useful referee opinion. At Warsaw, this work is supported through grants 2-P03D-014-07 and 2-P03D-005-16 of the Polish National Committee for Scientific Research. Also, J.A. and E.E. acknowledges support through Estonian SF grant 2446.

## REFERENCES

Alberts F., Savonije G. J., van den Heuvel E. P. J., Pols O. R., 1996, *Nature*, 380, 676  
 Alexander D. R., Ferguson J. W., 1994, *ApJ*, 437, 879  
 Benvenuto O. G., Althaus L. G., 1998, *MNRAS*, 293, 177: BA98  
 Bell J.F., Bailes M., Manchester R.N., Weisberg J.M., Lyne A.G., 1995, *ApJ*, 440, L81  
 Bergeron P., Weselmael F., Fontaine G., 1991, *ApJ*, 367, 253  
 Callanan P.J., Garnavich P.M., Koester D., 1998, *MNRAS*, 298, 207  
 Driebe T., Schönberner D., Blöcker T., Herwig F., 1998, *A&A*, 339, 123: DSB98  
 Ergma E., Sarna M. J., 1996, *MNRAS*, 280, 1000  
 Ergma E., Sarna M.J., Antipova J., 1998, *MNRAS*, 300, 352  
 Hamada T., Salpeter E. E., 1961, *ApJ*, 134, 683  
 Hansen B. M. S., Kawaler S., 1994, *Stellar interiors: Physical principals, structure and evolution*. A & A Library, Springer-Verlag, New York.  
 Hansen B. M. S., Phinney E. S., 1998a, *MNRAS*, 294, 557: HP98  
 Hansen B. M. S., Phinney E. S., 1998b, *MNRAS*, 294, 569  
 Huebner W. F., Merts A. L., Magee N. H. Jr., Argo M. F., 1977, *Astrophys. Opacity Library*, Los Alamos Scientific Lab. Report No. LA-6760-M  
 Iben I., Tutukov A. V., 1986, *ApJ*, 311, 742: IT86  
 Iglesias C. A., Rogers F. J., 1996, *ApJ*, 464, 943  
 Johnston S., et al., 1993, *Nature*, 361, 613  
 Joss P. C., Rappaport S., Lewis W., 1987, *ApJ*, 319, 180  
 Landau L. D., Lifshitz E. M., 1971, *Classical theory of fields*. Pergamon Press, Oxford  
 Lorimer D.R., Lyne A.G., Festin L., Nicastro L., 1995, *Nature*, 376, 393  
 Kippenhahn R., Kohl K., Weigert A., 1967, *ZAstrophys.*, 66, 58  
 Kippenhahn R., Thomas H.-C., Weigert A., 1968, *ZAstrophys.*, 68, 256  
 Mestel L., 1968, *MNRAS*, 138, 359  
 Mestel L., Spruit H. C., 1987, *MNRAS*, 226, 57  
 Muslimov A. G., Sarna M. J., 1993, *MNRAS*, 262, 164  
 Muslimov A. G., Sarna M. J., 1995, *ApJ*, 448, 289  
 Paczyński B., 1969, *Acta Astron.*, 19, 1  
 Paczyński B., 1970, *Acta Astron.*, 20, 47  
 Pols O. R., Tout Ch. A., Eggleton P. P., Han Z., 1995, *MNRAS*, 274, 964  
 Rappaport S., Podsiadlowski P., Joss P. C., Di Stefano R., Han Z., 1995, *MNRAS*, 273, 731  
 Refsdal S., Weigert A., 1971, *A&A*, 13, 367  
 Tauris T., 1996, *A&A*, 315, 453  
 Tout C. A., Hall D. S., 1991, *MNRAS*, 253, 9  
 Sandhu J. S., Bailes M., Manchester R.N., Navarro J., Kulkarni S.R., & Anderson S.B. 1997, *ApJ*, 478, L95  
 van Kerkwijk M. H., Bergeron P., Kulkarni S. R., 1996, *ApJ*, 467, L41  
 Webbink R. F., 1975, *MNRAS*, 171, 555: W75  
 Wood M. A., 1990, PhD thesis, The University of Texas at Austin  
 Ziolkowski J., 1970, *Acta Astron.*, 20, 59

Table 1a Cooling track characteristics

model	$P_i$ [days]	$M_i$ [ $M_\odot$ ]	$\lg t_{cool}$ [yrs]	$\lg t_{evol}$ [yrs]	$X_{surf}^f$	$P_f$ [days]	$M_f$ [ $M_\odot$ ]	$M_{2,He}(RLOF)$ [ $M_\odot$ ]	$M_{2,He}(COOL)$ [ $M_\odot$ ]	$\lg L_f$ [ $L_\odot$ ]	$\lg T_{eff,f}$
Z=0.003											
1	1.02	1.0	10.004	10.197	0.38	0.421	0.172	0.112	0.150	-2.299	3.920
2	1.05	1.0	9.948	10.159	0.39	0.554	0.175	0.115	0.152	-2.232	3.936
3	1.10	1.0	9.867	10.108	0.39	0.708	0.178	0.119	0.158	-2.139	3.959
4	1.30	1.0	9.685	10.008	0.40	1.180	0.187	0.134	0.169	-1.944	4.008
5	1.50	1.0	9.582	9.958	0.40	1.584	0.192	0.143	0.177	-1.843	4.035
6	2.00	1.0	9.399	9.885	0.41	2.614	0.203	0.160	0.189	-1.673	4.080
7	2.50 H	1.0	9.211	9.831	0.43	4.275	0.213	0.176	0.201	-1.499	4.125
8	3.00 H	1.0	9.107	9.809	0.44	5.498	0.219	0.185	0.207	-1.403	4.142
9	0.70	1.5	9.479	9.645	0.43	1.591	0.191	0.137	0.175	-1.659	4.066
10	0.80	1.5	9.122	9.474	0.44	2.092	0.199	0.146	0.184	-1.364	4.129
11	0.90	1.5	9.061	9.392	0.44	2.450	0.204	0.154	0.190	-1.201	4.165
12	1.20 H*	1.5	8.845	9.304	0.46	3.409	0.213/	0.169	0.200	-0.986	4.210
							0.212				
13	1.50 H*	1.5	8.788	9.286	0.48	4.280	0.217/	0.178	0.206	-0.929	4.224
							0.217				
14	1.80 H*	1.5	8.753	9.277	0.49	5.105	0.221/	0.185	0.210	-0.925	4.230
							0.221				
15	2.10 H*	1.5	8.766	9.283	0.49	5.866	0.225/	0.192	0.214	-0.957	4.229
							0.224				
16	2.50 H*	1.5	8.742	9.278	0.48	6.831	0.229/	0.197	0.219	-0.976	4.232
							0.228				
17	3.00 H*	1.5	8.665	9.259	0.49	7.888	0.232/	0.203	0.223	-1.010	4.231
							0.231				
Z=0.01											
18	1.30	1.0	10.212	10.388	0.38	0.366	0.163	0.120	0.143	-2.601	3.847
19	1.35	1.0	9.907	10.316	0.39	0.605	0.168	0.127	0.150	-2.477	3.877
20	1.45	1.0	9.886	10.193	0.40	1.092	0.177	0.139	0.161	-2.231	3.934
21	1.65	1.0	9.661	10.094	0.42	1.945	0.188	0.154	0.175	-1.995	3.993
22	2.00 H*	1.0	9.490	10.037	0.43	2.936	0.197/	0.166	0.185	-1.829	4.035
							0.196				
23	2.50 H*	1.0	9.165	9.967	0.45	4.272	0.205/	0.173	0.194	-1.606	4.085
							0.203				
24	3.00 H*	1.0	9.152	9.965	0.45	5.546	0.211/	0.184	0.201	-1.546	4.104
							0.209				
25	0.90	1.5	9.902	10.007	0.44	1.075	0.174	0.132	0.156	-2.168	3.937
26	1.05	1.5	9.650	9.810	0.47	1.855	0.186	0.148	0.172	-1.872	4.008
27	1.10	1.5	9.596	9.772	0.46	2.032	0.188	0.152	0.175	-1.832	4.020
28	1.20	1.5	9.504	9.710	0.47	2.378	0.192	0.157	0.180	-1.741	4.042
29	1.50 H*	1.5	9.368	9.629	0.47	3.152	0.200/	0.169	0.188	-1.645	4.069
							0.199				
30	2.00 H*	1.5	9.273	9.578	0.48	4.153	0.206/	0.178	0.195	-1.572	4.091
							0.205				
31	2.50 H*	1.5	9.111	9.505	0.49	5.091	0.211/	0.185	0.201	-1.475	4.114
							0.209				
32	3.00 H*	1.5	9.091	9.501	0.50	7.896	0.221/	0.197	0.213	-1.455	4.130
							0.221				

Table 1b Cooling track characteristics

model	$P_i$ [days]	$M_i$ [ $M_\odot$ ]	$\lg t_{cool}$ [yrs]	$\lg t_{evol}$ [yrs]	$X_{surf}^f$	$P_f$ [days]	$M_f$ [ $M_\odot$ ]	$M_{2,He}(RLOF)$ [ $M_\odot$ ]	$M_{2,He}(COOL)$ [ $M_\odot$ ]	$\lg L_f$ [ $L_\odot$ ]	$\lg T_{eff,f}$
Z=0.02											
33	1.20	1.0	10.237	10.467	0.37	0.416	0.162	0.128	0.145	-2.673	3.830
34	1.50	1.0	9.850	10.277	0.41	1.489	0.179	0.149	0.166	-2.245	3.929
35	2.00 H*	1.0	9.582	10.193	0.43	2.912	0.192/	0.164	0.181	-1.978	3.995
							0.191				
36	2.50 H*	1.0	9.420	10.159	0.45	4.242	0.200/	0.175	0.190	-1.819	4.033
37	3.00 H*	1.0	9.299	10.139	0.47	5.551	0.206/	0.182	0.196	-1.698	4.062
							0.205				
38	1.20	1.5	10.168	10.255	0.44	0.736	0.170	0.141	0.155	-2.570	3.854
39	1.50	1.5	9.835	9.987	0.44	1.737	0.183	0.154	0.171	-2.198	3.939
40	2.00 H*	1.5	9.448	9.747	0.48	4.230	0.203/	0.179	0.193	-1.831	4.032
							0.202				
41	2.50 H*	1.5	9.295	9.677	0.49	5.910	0.210/	0.188	0.202	-1.690	4.067
42	3.00 H*	1.5	9.074	9.599	0.52	7.686	0.216/	0.196	0.209	-1.537	4.100
							0.215				
Z=0.03											
43	1.15	1.0	10.287	10.553	0.37	0.305	0.160	0.130	0.143	-2.753	3.809
44	1.30	1.0	10.104	10.462	0.38	0.882	0.169	0.140	0.156	-2.562	3.856
45	1.50	1.0	9.909	10.384	0.40	1.488	0.177	0.149	0.166	-2.343	3.906
46	1.65	1.0	9.809	10.353	0.41	1.884	0.182	0.156	0.171	-2.242	3.930
47	1.80 H*	1.0	9.693	10.323	0.41	2.303	0.185/	0.160	0.175	-2.149	3.950
							0.184				
48	2.50 H*	1.0	9.474	10.281	0.45	4.222	0.197/	0.175	0.188	-1.912	4.008
49	3.00 H*	1.0	9.366	10.265	0.47	5.541	0.203/	0.181	0.195	-1.798	4.035
							0.202				
50	1.35	1.5	10.264	10.353	0.42	0.497	0.165	0.137	0.150	-2.694	3.822
51	1.50	1.5	10.045	10.173	0.42	1.190	0.174	0.146	0.161	-2.464	3.876
52	1.70	1.5	9.829	10.015	0.42	1.968	0.184	0.156	0.173	-2.246	3.929
53	1.80 H*	1.5	9.580	9.873	0.46	3.380	0.196/	0.174	0.187	-2.020	3.984
							0.194				
54	2.50 H*	1.5	9.353	9.772	0.49	5.850	0.208/	0.188	0.200	-1.801	4.039
55	3.00 H*	1.5	9.151	9.705	0.51	7.671	0.214/	0.195	0.207	-1.651	4.073
							0.213				

Listed are:

 $P_i$  is initial orbital period of the system (at the beginning of mass transfer) $M_i$  is the mass of the progenitor of white dwarf $t_{cool}$  is duration of the cooling phase of a white dwarf starting at the end of RLOF $t_{evol}$  is total evolution time $X_{surf}^f$  is the final surface hydrogen content $P_f$  is final orbital period at the moment of shrinking of the donor within its Roche lobe $M_f$  is final WD mass $M_{2,He}(RLOF)$  is the mass of the helium core at the moment of shrinking of the donor within its Roche lobe $M_{2,He}(COOL)$  is the final mass of helium core after the central temperature has decreased by 50% of its maximum value $L_f$  is the final luminosity $T_{eff,f}$  is the final effective temperature.

H - hydrogen flashes without RLOF

H\* - hydrogen flashes with RLOF

Table 2 M-R relation for a cooling low-mass WD with a helium core

$M_{\text{wd}}/M_{\odot}$	$R_0/R_{\odot}$	$R_{8500}/R_0$	$R_{8500}/R_0$	$\log g_1$	$R_{8500}/R_0$	$\log g_2$
0.155	0.0218	2.100	-	6.31	1.351	6.69
0.180	0.0208	1.594	1.687	6.65	1.300	6.82
0.206	0.0198	1.469	1.476	6.83	1.236	7.00
0.296*	0.0173	1.224	1.220	7.26	1.111	7.36

The first two columns present the zero-temperature M-R relation for a helium WD obtained by Hamada & Salpeter (1961). The third and fifth columns display our calculations of the stellar radius and gravity, while fourth and fifth the DSBH98 calculations, respectively. The last two columns illustrate the same quantities taken from the cooling tracks produced by Wood (1990) for carbon WDs with thick hydrogen envelopes. The stellar radius is calculated at  $T = 8500$  K and is normalized by the zero-temperature radius.

\*the last two values in this row are taken from IT86.

Table 3 Comparison of the cooling time-scales of  
HP98, BA98 and Webbink, ours models

		HP98 and BA98	Webbink and ours
$M_{\text{He}}/M_{\odot}$	$\log L/L_{\odot}$	$t_{\text{cool}}$ (Gyrs)	$t_{\text{cool}}$ (Gyrs)
0.15	-3.1	1.0	36.4
0.25	-2.9	1.0	6.1
0.30	-2.9	1.0	4.2

Table 4a Flash characteristics

model	case	$\lg \Delta t_1$ [yrs]	$\lg \Delta t_{acc}$ [yrs]	$\lg \Delta t_2$ [yrs]	$\lg \Delta T$ [yrs]	$\lg L_{max}/L_\odot$	$\lg T_{eff}$ [ $L=L_{max}$ ]	$M_{b,env}$ [ $M_\odot$ ]	$M_{a,env}$ [ $M_\odot$ ]	$\Delta M_{acc}$ [ $\times 10^{-4} M_\odot$ ]
7	1	6.377		6.349	6.595	0.526	4.349			
	1	6.852		6.599	6.450	1.525	4.117			
	1	7.095		6.609	6.584	1.603	4.073			
	1	7.346		6.598		1.693	4.011			
8	1	6.453		6.509	6.520	1.571	4.147			
	1	6.906		6.580	6.553	1.658	4.084			
	1	7.183		6.596		1.740	4.037			
12	1	6.634		6.551	6.484	0.912	4.330			
	1	6.907		6.608	6.449	1.548	4.084			
	1	7.139		6.601	6.649	1.619	4.044			
	2	7.367	2.673	6.456		1.703	4.015	0.0129	0.0123	1.7
13	1	6.717		6.590	6.474	1.577	4.099			
	1	6.971		6.612	6.574	1.646	4.053			
	2	7.215	2.192	6.571		1.727	3.979	0.0119	0.0118	0.2
14	1	6.372		6.519	6.473	1.588	4.119			
	1	6.861		6.585	6.475	1.670	4.078			
	1	7.141		6.588	7.603	1.751	3.994			
	2	6.435	2.593	6.258		1.843	3.982	0.0113	0.0105	3.5
15	1	6.538		6.558	6.443	1.669	4.099			
	1	6.975		6.567	6.516	1.748	4.038			
	2	7.283	2.433	6.450		1.842	3.963	0.0108	0.0103	1.2
16	1	6.643		6.551	6.462	1.757	4.082			
	1	7.091		6.553	6.622	1.846	4.016			
	2	7.501	2.513	6.172		1.965	3.983	0.0100	0.0095	4.4
17	1	5.774		6.646	6.510	1.829	4.047			
	2	7.202	2.272	6.477	6.723	1.933	3.940	0.0120	0.0094	0.6
	2	7.688	2.389	5.931		2.094	3.983	0.0094	0.0082	8.2
22	1	6.495		6.513	6.674	0.312	4.253			
	2	7.029	3.154	6.113		1.311	3.938	0.0121	0.0116	4.7
23	2	6.998	2.994	6.124	6.884	1.459	3.922	0.0115	0.0105	4.9
	2	7.902	2.806	5.915		1.679	3.975	0.0105	0.0088	14.1
24	2	6.823	2.914	6.171	6.801	1.546	3.914	0.0103	0.0097	3.9
	2	7.623	2.769	5.966		1.695	3.939	0.0097	0.0086	10.4
29	1	6.662		6.583	6.634	0.371	4.246			
	2	6.971	3.177	5.984		1.307	3.293	0.0120	0.0108	6.2
30	2	6.880	3.066	5.967		1.412	3.918	0.0112	0.0100	5.7
31	2	6.652	2.994	6.011	6.793	1.470	3.906	0.0103	0.0095	4.3
	2	7.666	2.843	5.899		1.641	3.955	0.0095	0.0083	11.6
32	2	7.005	2.779	5.825		1.682	3.900	0.0090	0.0078	7.9

Table 4b Flash characteristics

model	case	$\lg \Delta t_1$ [yrs]	$\lg \Delta t_{acc}$ [yrs]	$\lg \Delta t_2$ [yrs]	$\lg \Delta T$ [yrs]	$\lg L_{max}/L_\odot$	$\lg T_{eff}$ [ $L=L_{max}$ ]	$M_{b,env}$ [ $M_\odot$ ]	$M_{a,env}$ [ $M_\odot$ ]	$\Delta M_{acc}$ [ $\times 10^{-4} M_\odot$ ]
35	1	6.510		6.425	6.799	-0.068	4.205			
	2	6.864	3.290	5.969		1.173	3.911	0.0111	0.0102	7.4
36	2	6.720	3.158	5.850		1.313	3.897	0.0102	0.0089	8.6
37	2	6.885	2.999	5.810		1.419	3.877	0.0097	0.0082	10.5
40	2	6.622	3.168	5.549		1.275	3.883	0.0098	0.0084	9.2
41	2	6.876	2.981	5.719		1.427	3.875	0.0087	0.0076	10.2
42	2	7.362	2.744	5.737		1.615	3.876	0.0079	0.0063	11.6
47	1	7.373		6.594	6.966	0.208	4.151			
	2	6.095	3.388	5.938		1.072	3.926	0.0109	0.0095	12.7
48	2	6.809	3.200	5.820		1.239	3.864	0.0094	0.0080	11.1
49	2	6.871	3.081	5.836		1.317	3.863	0.0089	0.0074	9.9
53	1	6.471		6.690	6.819	0.190	4.170			
	2	6.920	3.239	6.785		1.160	3.889	0.0094	0.0078	12.4
54	2	6.927	2.962	5.722		1.355	3.855	0.0081	0.0066	11.1
55	2	7.180	2.785	5.734		1.521	3.849	0.0074	0.0058	11.8

Listed are:

number of model (Table 1)

number of case (1 or 2)

$\Delta t_1$  and  $\Delta t_2$  are the rise and decay times respectively

$\Delta T$  and  $\Delta t_{acc}$  are recurrence time between two successful flashes and duration of accretion phase during the flash

$T_{eff}$  is effective temperature when the luminosity has its maximum value  $L_{max}$

$M_{b,env}$  and  $M_{a,env}$  are the envelope masses before and after flash

$\Delta M_{acc}$  is accreted mass

$M_{b,env} - M_{a,env} = \Delta M_{He,c} + \Delta M_{acc}$  where  $\Delta M_{He,c}$  is the increase of the helium core mass during the flash.

